



**CASE FILE
COPY**

**DEVELOPMENT OF A SINUSOIDAL PRESSURE
GENERATOR FOR PRESSURE TRANSDUCER
DYNAMIC CALIBRATION**

by

Richard E. Robinson

Prepared for

NATIONAL AERONAUTICS AND SPACE ADMINISTRATION

NASA Lewis Research Center
Contract NAS 3-11229
Richard J. Priem, Project Manager
Chemical Rocket Division
Marshall C. Burrows, Technical Monitor
Physics & Chemistry Division

**BATTELLE MEMORIAL INSTITUTE
COLUMBUS, OHIO**

NOTICE

This report was prepared as an account of Government-sponsored work. Neither the United States, nor the National Aeronautics and Space Administration (NASA), nor any person acting on behalf of NASA:

- (A) Makes any warranty or representation, expressed or implied, with respect to the accuracy, completeness, or usefulness of the information contained in this report, or that the use of any information, apparatus, method, or process disclosed in this report may not infringe privately-owned rights; or
- (B) Assumes any liabilities with respect to the use of, or for damages resulting from the use of, any information, apparatus, method or process disclosed in this report.

As used above, "person acting on behalf of NASA" includes any employee or contractor of NASA, or employee of such contractor, to the extent that such employee or contractor of NASA or employee of such contractor prepares, disseminates, or provides access to any information pursuant to his employment or contract with NASA, or his employment with such contractor.

Requests for copies of this report should be referred to

National Aeronautics and Space Administration
Scientific and Technical Information Facility
P. O. Box 33
College Park, Maryland 20740

INTERIM REPORT

DEVELOPMENT OF A SINUSOIDAL PRESSURE GENERATOR
FOR PRESSURE TRANSDUCER DYNAMIC CALIBRATION

by

Richard E. Robinson

Prepared for

NATIONAL AERONAUTICS AND SPACE ADMINISTRATION

March 25, 1970

Contract NAS 3-11229

Technical Management
NASA Lewis Research Center
Cleveland, Ohio
Marshall C. Burrows

BATTELLE MEMORIAL INSTITUTE
Columbus Laboratories
505 King Avenue
Columbus, Ohio 43201

FOREWORD

This report summarizes the efforts performed by Battelle's Columbus Laboratories under NASA Contract No. NAS 3-11229 from June, 1968 through August, 1969. The project manager was Dr. Richard J. Priem, Chemical Rocket Division, and the technical monitor was Dr. Marshall C. Burrow, Physics and Chemistry Division, National Aeronautics and Space Administration, Lewis Research Center, Cleveland, Ohio 44135.

The author wishes to acknowledge the contribution of several individuals to the work described in the report. Dr. C. Y. Liu advised throughout the program, Mr. W. H. Wilkinson performed design analyses, and Dr. E. W. Ungar acted in a supervisory capacity.

TABLE OF CONTENTS

	<u>Page</u>
SUMMARY	1
INTRODUCTION.	1
LIST OF SYMBOLS	3
THEORY AND DEVELOPMENT OF AN INLET-MODULATED SINUSOIDAL PRESSURE GENERATOR	5
Principle of Operation	5
Design	7
Analytical Design	7
Mechanical Design14
IM-SPG CHARACTERIZATION SETUP17
Description of System and Operation.17
Instrumentation and Data Recording20
IM-SPG CHARACTERIZATION RESULTS21
Inlet Pressure to Average Chamber Pressure Ratio21
Oscillating Pressure Amplitude22
Waveform24
SUMMARY OF RESULTS.29
RECOMMENDATIONS30
REFERENCES.31

APPENDIX A

DERIVATIONS OF EQUATIONS GOVERNING THE OPERATION OF THE SINUSOIDAL PRESSURE GENERATOR.	A-1
---	-----

APPENDIX B

APPROXIMATE SOLUTION ACCURACY	B-1
---	-----

LIST OF TABLES

	<u>Page</u>
TABLE 1. CALCULATED HOLE SIZES	12
TABLE 2. CALCULATED PEAK-TO-PEAK PRESSURE.	12
TABLE 3. TEST CONDITIONS	28

LIST OF FIGURES

FIGURE 1. INLET-MODULATED SINUSOIDAL PRESSURE GENERATOR.	6
FIGURE 2. PERCENT PEAK-TO-PEAK PRESSURE TO CHAMBER PRESSURE VERSUS FREQUENCY FOR INLET-MODULATED SPG.	13
FIGURE 3. DRAWING OF INLET-MODULATED SINUSOIDAL PRESSURE GENERATOR	15
FIGURE 4. SINUSOIDAL PRESSURE GENERATOR.	18
FIGURE 5. SCHEMATIC OF SINUSOIDAL PRESSURE GENERATOR SYSTEM. . . .	19
FIGURE 6. EXPERIMENTAL SINUSOIDAL PRESSURE GENERATOR PERFORMANCE .	23
FIGURE 7. TYPICAL PRESSURE HISTORIES AT LOW FREQUENCIES AT VARIOUS PRESSURE LEVELS.	25
FIGURE 8. TYPICAL PRESSURE HISTORIES AT MEDIUM FREQUENCIES AT VARIOUS PRESSURE LEVELS.	26
FIGURE 9. TYPICAL PRESSURE HISTORIES AT HIGH FREQUENCIES AT VARIOUS PRESSURE LEVELS.	27
FIGURE A-1. INLET-MODULATED SINUSOIDAL PRESSURE GENERATOR.	A-1

ABSTRACT

The purpose of this effort was to develop a new sinusoidal pressure generator for use in the dynamic calibration of pressure transducers and to evaluate the performance of the device. Evaluation tests were conducted using two different performance settings at chamber pressures up to 300 psia (2070 kN/m²-abs) and over a frequency range of 1-15 kHz. Specified oscillation pressure amplitude performance was exceeded by 50 percent. Excellent agreement between the theoretical-predicted pressures and those obtained experimentally was found. It was concluded that the unit is suitable for dynamic response evaluation of pressure sensing systems over a wide range of pressure levels, amplitudes, and frequency.

DEVELOPMENT OF A SINUSOIDAL PRESSURE
GENERATOR FOR PRESSURE TRANSDUCER
DYNAMIC CALIBRATION

by Richard E. Robinson

SUMMARY

Development and initial performance tests of a sinusoidal pressure generator for the dynamic calibration of pressure transducers have been completed and the results are presented. The generator is an inlet-area-modulated, gas-flow-through device. Theoretical performance for the six possible operating modes is given. Experimental performance over a frequency range of 1 to 15 kilohertz for the two modes tested are presented. Predicted performance was achieved experimentally. Sinusoidal peak-to-peak pressures of 120 percent, 18 percent and 12 percent of bias pressures were obtained at 1, 10, and 15 kilohertz, respectively, for one mode while 10 percent at 10 kilohertz and 6 percent at 15 kilohertz were obtained for the other mode. Higher and lower percentages are predicted for the remaining modes. Waveform oscillographs of filtered and unfiltered pressure transducer output signals are presented and discussed.

INTRODUCTION

The need to obtain reliable dynamic pressure measurements has resulted in the requirement to develop suitable dynamic instrument calibration procedures. Much of the early dynamic pressure measurement efforts were associated with the measurement of high-frequency combustion instability phenomena in rocket engines. More recently, the rocket engine development requirement has been complemented by development requirements for advanced aircraft engines. These new requirements include the quieting of engines and body-fan-engine interferences. New technology such as fluidics have also added to the need as has the upgrading of technology in fields such as internal combustion engine development programs.

The dynamic performance characteristics of pressure transducers and pressure measuring systems can be directly determined by a sinusoidal pressure calibrator. Battelle-Columbus studied methods for generating large-amplitude, high-frequency pressure fluctuations at high average static pressures such as those encountered in rocket motor combustion instabilities(1)*. The results of the methods study were that a Battelle concept--an inlet-area-modulated, gas-flow-through device (siren type)--showed the most potential for advancing the state of the art. An analytical and experimental investigation was made

* Numbers in parentheses refer to references listed at the end of this report.

of the inlet-modulated design concept to determine its feasibility, performance, and its applicability to dynamic pressure transducer evaluations at pressure conditions of interest. The experimental investigation was performed by modifying an outlet-modulated, Princeton University Sinusoidal Pressure Generator. The tests established the inlet-modulated sinusoidal pressure generator concept as feasible and applicable to transducer evaluations.

The above work tested the concept by temporarily modifying a generator from the NASA dynamic pressure evaluation equipment presently located at Battelle's Columbus Laboratories. In order to utilize the new calibration technology, the present work was undertaken to design, construct, and evaluate an inlet-modulated sinusoidal pressure generator (IM-SPG).

The specified performance of the IM-SPG was that it was to be capable of operating at mean pressures from 15 psia ($103.5 \text{ kN/m}^2\text{abs}$) to 1500 psia ($10.35 \text{ MN/m}^2\text{abs}$) over a frequency range of 15 Hertz to 15,000 Hertz with ratios of peak-to-peak pressure amplitude to average pressure of 1.0 at 15 Hertz and 0.12 at 10,000 Hertz.

In addition, the unit was to be designed for hydrogen operation. Hydrogen offers higher frequency and better waveshape capability because of its higher speed of wave propagation (speed of sound). The dynamic pressure at a given frequency and average chamber pressure is also highest for hydrogen because it is a function of the gas constant and the specific heat ratio. The cost of hydrogen is lower than nitrogen and helium, the two gases most commonly used in this type of generator. Hydrogen has the major disadvantage of being hazardous and, therefore, requiring special handling and design precautions.

LIST OF SYMBOLS

- A = Area
- A_{B_j} = j additional inlets
- A_{B_k} = k additional outlets
- A_I = Total physical area of flow passage
- C = Speed of sound
- C_D = Discharge coefficient
- d = Diameter
- f = Frequency
- g_c = Unit conversion factor = $32.17 \frac{\text{lb}_m \cdot \text{ft}}{\text{ft} \cdot \text{lbm} \cdot \text{sec}^2}$
- $K = \sqrt{\frac{\gamma}{R} \left(\frac{2}{\gamma+1}\right)^{\frac{\gamma+1}{\gamma-1}}}$
- \dot{m} = Mass flow rate
- p = Pressure
- $\hat{p} = 2 \frac{\tilde{p}}{p} = \frac{\text{peak-to-peak pressure}}{\text{average chamber pressure}}$
- P_I = Inlet pressure = supply pressure
- R = Gas constant
- T = Temperature
- V = Volume
- $\alpha = \left[\frac{g_c \gamma}{RT_o} \left(\frac{2}{\gamma+1}\right)^{\frac{\gamma+1}{\gamma-1}} \right]^{1/2}$
- γ = Ratio of specific heats
- ϵ = Error

$$\eta = \frac{\alpha RT_o}{V}$$

$\omega = 2\pi f = \text{angular frequency}$

Subscripts

amp = Relates to amplitude of variable

c = Chamber

e = Exit

i = Inlet

o = Gas stagnation conditions

t = Throat

Superscripts

. = Derivative with respect to time

* = Ratio with respect to p_o

- = Average portion

~ = Fluctuation portion

THEORY AND DEVELOPMENT OF AN INLET MODULATED
SINUSOIDAL PRESSURE GENERATOR

Principle of Operation

Pressure oscillations in this type of generator are produced by controlling the gas flow into and out of a chamber. The pressure in the chamber is sensed by the test transducer and by a standard transducer. Sinusoidal pressure variation is obtained by varying the mass flow through the chamber in a sinusoidal manner (assuming linear flow phenomena) as a function of time. The IM-SPG is a fixed volume-variable mass or flow-modulated SPG.

The pressure level in the chamber is used for calibration purposes rather than the exhaust pressure. The exhaust (like a siren) although sinusoidal initially, degenerates into the common N-wave or sawtooth wave-shape because of the nonlinearities associated with large-amplitude, high-frequency wave propagation phenomena. Normally, eight to ten wavelengths travel are required for a propagating large amplitude sine wave to fully develop into an N-wave. Pressure differences across the chamber are minimized by keeping the chamber dimensions smaller than the wavelength of the sinusoidal oscillation being generated. Thus, pressure wave propagation phenomenon is minimal because it cannot develop much in less than a wavelength--the chamber pressure change is essentially quasi-steady and is an expansion-compression phenomenon.

In its simplest form the generator consists of a cylindrical chamber with a modulated inlet flow opening and a fixed outlet flow opening. Although the two flow openings could be located through any surface, they are usually placed on the curved or side surfaces (diametrically opposite each other). The flat or end surfaces are used for placing the pressure transducer or measuring system under evaluation. The required mass flow variation is achieved by operating the flow openings or nozzles at supercritical flow conditions and varying the area. Nozzle discharge coefficients are essentially constant above critical conditions and most importantly flow is independent of downstream pressure conditions as long as they are below the critical pressure ($\sim 1/2$ the upstream pressure for most gases). The mass flow is directly proportional to the flow cross-sectional area for any gas at fixed upstream pressure and temperature. This relationship is expressed by:

$$\dot{m} = \frac{C_D K p_o A}{\sqrt{T_o}}, \quad (1)$$

where

$$K = \sqrt{\frac{\gamma}{R} \left(\frac{2}{\gamma+1} \right)^{\frac{\gamma+1}{\gamma-1}}} \quad (2)$$

Thus, sinusoidal mass flow into or out of the chamber can be accomplished by varying or modulating the inlet area sinusoidally and maintaining critical flow.

Area variation is achieved by rotating a circular disk with numerous holes located along a circle near the disc periphery against the inlet nozzle throat. The holes in the disk are the same size (diameter) and shape (circular) as the nozzle throat. They are equally spaced one hole diameter apart on a hole-circle near the periphery of the disk. Rotation of the wheel alternately blocks and opens the flow area. Although the passage of a circular hole past a circular nozzle throat is not exactly a sinusoidal area change⁽²⁾, various nonlinear flow effects associated with the clearance between the nozzle throat and disk, and contraction and expansion phenomena cause the final chamber pressure variation to closely approximate sinusoidal oscillations.

The above two-hole concept was extended during the work reported by Reference 1. A third hole acting as an inlet was proposed. The third hole was not modulated and allowed independent control of the average chamber or bias pressure and the dynamic pressure amplitude at any frequency. During the present work the concept was further extended to N additional holes. Any number of the N-number of unmodulated holes could be used and in any combination of inlet or outlet flow passages. Independent control of each inlet mass flow (always above critical pressure) further extends the achievable pressure conditions. Appendix A presents a first order examination of the phenomena associated with the IM-SPG.

The inlet-modulated design concept is shown in Figure 1.

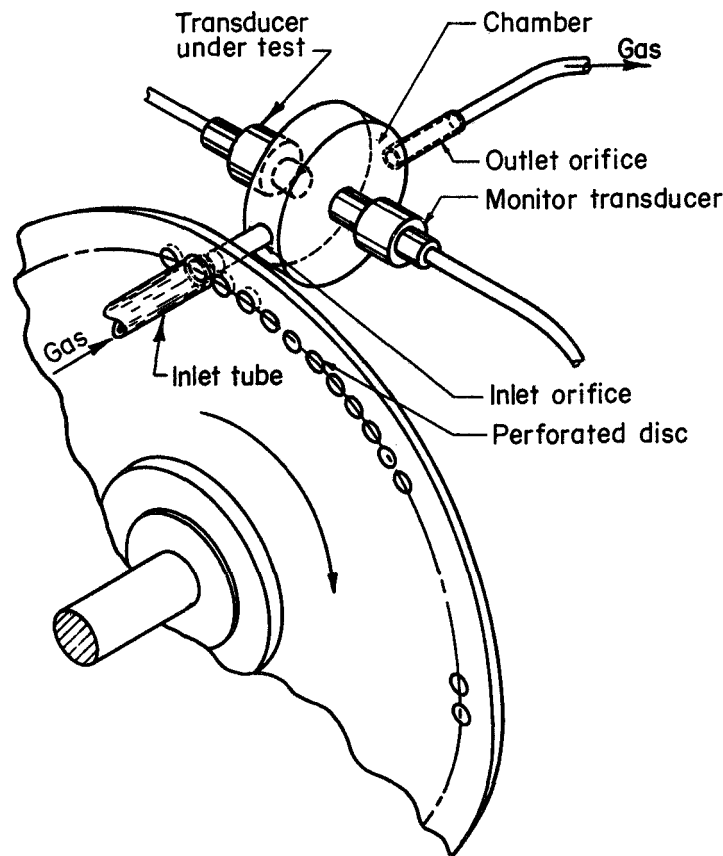


FIGURE 1. INLET-MODULATED SINUSOIDAL PRESSURE GENERATOR

Design

As a first step in the design of the IM-SPG a study of latest company catalogs and instrumentation reports on dynamic pressure transducers and measurements was made. The study was performed to determine the size ranges and characteristics of transducers available and currently in use. Frequency of use considerations were determined by a telephone survey of many of the government facilities and transducer manufacturers. From these studies, two chamber sizes were selected as bounds for the initial analytical and mechanical design analyses, 3/4-inch (19.1 mm) and 3/8-inch (9.5 mm) diameter.

The 3/4-inch (19.1 mm) diameter chamber was selected for development first because its size allowed full development of the inlet-modulated concepts, without introducing severe scaling considerations initially. The previously available outlet-modulated SPG has a 3/4-inch (19.1 mm) diameter chamber. Thus, the effects of disk-to-chamber nozzle clearances of the order of a thousandth of an inch (0.025 mm) on a 3/4-inch (19.1 mm) diameter chamber are known. Similarly, nozzle sizes and the nozzle-to-chamber relationship would be essentially the same again eliminating scaling of complex fluid dynamic phenomena, e.g., nozzle throat and expansion area boundary layers and shock considerations. Clearances of the same order are about all that could be practically obtained with a 3/8-inch (9.5 mm) diameter. The effects of the proportionately larger clearance ratios are not known.

Analytical Design

Following the selection of chamber dimensions analyses were performed to determine the SPG parts sizes and tolerances to produce the specified performance.

General. Maintenance of chamber dimensions smaller than the shortest wavelength of the sinusoidal pressure oscillation of concern assures that this oscillation frequency is less than the resonant frequency of the chamber. The tangential modes of oscillations are the first to appear in cylinders with a length-to-diameter ratio of less than 1.71.⁽³⁾ Not only is the tangential mode resonant frequency higher than the first longitudinal or the first radial mode resonant frequencies for each diameter but the tangential modes should not affect the response of transducers mounted on the cylinder ends⁽³⁾. In light of these considerations a length-to-diameter ratio of 0.35 was chosen for the 3/4-inch (19.1 mm) diameter chamber previously selected.

Equations (1) and (2) and (A-11) and (A-12) from Appendix A express the various relationships between performance and chamber parameters. Examination of these expressions gives the various characteristics of the SPG. The characteristics and the design guidelines employed are discussed next.

The sinusoidal pressure variation is caused by mass additions to and subtractions from the chamber. The mass required (per cycle) increases with chamber volume—regardless of the pressure conditions (\bar{p} or \bar{p}). The mass flow rates (at each frequency) increases with \bar{p} and \bar{p} and increases with frequency. The use of critical flow nozzles to control these mass flows are desired for better control and to minimize flow disturbances in the chamber.

A nozzle has its flow controlling area (throat) smaller than its exit area. The chamber length is the largest the nozzle exit diameter can be. Thus, decreasing chamber length decreases the volume and mass requirements but also decreases nozzle exit and throat area. Decreasing of throat area increases the upstream (supply) pressure required for a given mass flow.

Two desirable features are that the inlet pressure be as low as possible and that the frequency range of an inlet nozzle be as large as possible. Low inlet pressure is desirable because it allows more tests from a given blowdown gas supply system pressure level and reduces pressure level requirements. Therefore, costs on the components such as regulators, lines, tanks, and gages as well as on commercial gas cylinders are also lower. A large frequency range for an inlet nozzle is desirable to reduce the number of precision machined rotating disks required (one for each throat size) and to avoid the delay of changing disks during a calibration series. Since the mass flow rate is directly proportional to both pressure and frequency range, they affect each other. Unfortunately, they affect each other adversely. A wide frequency range and an associated large amplitude at low frequencies requires a large nozzle area ratio. The larger the area ratio the smaller the throat will be, even if the maximum exit area (diameter equal to chamber length) is taken. The smaller the throat the higher the inlet pressure must be for a given mass flow rate or performance condition.

The outlet-modulated SPG (OM-SPG) developed by Princeton was found to have the best waveform with the critical flow inlet orifice operating with subsonic exit flow. This condition occurs when the supersonic flow downstream of the throat is overexpanded and shocks are formed within the nozzle which produce subsonic flow at the nozzle exit. The nozzle area ratio (exit to throat) must be sufficient to contain the shock between the throat and the exit over the range of pressure (chamber average plus fluctuation pressure) of the unit. The pressure available with the unit varies rather significantly with frequency. The fluctuation pressure varies in a manner which is nearly inversely proportional to frequency. For instance, the chamber pressure (inlet nozzle exhaust conditions) of the OM-SPG varies from $(1 \pm 0.5) P_c$ at 200 hertz to $(1 \pm 0.025) P_c$ at 10,000 hertz. The bias pressure remains essentially constant with P_c frequency. The larger the pressure range (and, therefore, frequency range) a nozzle must operate within, the smaller the critical throat must be relative to the maximum nozzle exit diameter which is the chamber length.

The IM-SPG was designed to meet performance specifications using hydrogen as a working gas. Because of the many interacting factors such as just described emphasis was placed on certain parameters at the expense of others. High amplitude at high frequency was given top priority even at the expense of waveshape. A wide frequency range was desired, preferably from several thousand Hertz up to 15,000 Hertz with one nozzle setting--again at the expense of waveshape if necessary. Finally, the bias pressure range from 50 psia (345 kN/m²abs) to 300 psia (2.07 MN/m²abs) was chosen for experimental evaluation, rather than 1500 psia (10.35 MN/m²abs).

Performance Analysis. The IM-SPG performance is determined by use of Equations (A-7) and (A-11) or alternately (A-7) and (A-12). Appendix B describes the criterion for choosing between Equations (A-11) or (A-12). Thus, based on Equation (A-11),

$$\frac{\tilde{p}_{amp}}{\bar{p}} = \frac{\tilde{\bar{A}}_i(amp)}{\left(A_e^2 + \frac{\omega^2}{\eta^2}\right)^{\frac{1}{2}} \bar{A}_i/A_e} = \frac{\tilde{\bar{A}}_i(amp)}{\left(1 + \frac{\omega^2}{A_e^2 \eta}\right)^{\frac{1}{2}} \bar{A}_i} \quad (3)$$

Alternately, based on Equation (A-12),

$$\frac{\tilde{p}_{amp}}{\bar{p}} = \frac{\eta \tilde{\bar{A}}_i}{\omega} / \frac{\bar{A}_i(amp)}{A_e} \quad (4)$$

The area variation of the circular disk hole past the circular nozzle throat is approximated by

$$\begin{aligned} A_i &= \frac{A_I}{2} (1 + \cos \omega t) \\ &= \frac{A_I}{2} + \frac{A_I}{2} \cos \omega t \end{aligned} \quad (5)$$

Here the first term contributes to the bias or average pressure and is included as part of \bar{A}_i and the second term contributes to the pressure variation and corresponds to A_i . A_I is the total area of the disk hole or inlet nozzle throat area. Thus, the terms in (A-6) are

$$\tilde{\bar{A}}_i = \frac{A_I}{2} \quad (6)$$

$$\bar{A}_i = \frac{A_I}{2} + \sum_{j=1}^{j=n} A_{B_j} \quad (7)$$

and therefore (A-7) is

$$A_e + \sum_{k=1}^{k=n} A_{B_k} = \frac{\bar{A}_i}{\bar{p}} = \frac{\frac{A_I}{2} + \sum_{j=1}^{j=n} A_{B_j}}{\bar{p}} \quad (8)$$

when A_{B_j} and A_{B_k} are additional inlets and outlets, respectively, for changing chamber bias pressure.

For hydrogen

$$\eta_{H_2} = \frac{C}{V} \left(\frac{2}{\gamma+1} \right)^{\frac{\gamma+1}{2(\gamma-1)}} = \frac{12 \sqrt{1.41 \times 32.2 \times 767 \times 500}}{0.262 \times \frac{\pi}{4} (0.75)^2} \left(\frac{2}{1.41+1} \right)^{\frac{1.41+1}{2(1.41-1)}}$$

$$= 2.5 \times 10^5 / \text{in.}^2\text{-sec} \quad (0.39 \times 10^3 / \text{mm}^2\text{-sec})$$

Substitution of η_{H_2} , (6), and (8) into (4) gives for one inlet and one outlet ($A_{B_j} = A_{B_k} = 0$) and changing from areas to diameters

$$\frac{\tilde{p}}{\bar{p}} = \frac{2.5 \times 10^5}{2\pi f} \times \frac{\pi}{4} \frac{d_{I/2}^2 d_e^2}{d_{I/2}^2} = \frac{3.12 \times 10^4}{f} d_e^2 \quad (9)$$

Letting

$$\frac{\hat{p}}{\bar{p}} = \frac{\text{peak-to-peak pressure}}{\text{average chamber pressure}} = 2 \frac{\tilde{p}}{\bar{p}} \quad (10)$$

Then for $f = 10,000$ Hz

$$\frac{\hat{p}}{\bar{p}} = 6.24 d_e^2$$

Solving for d_e to achieve the specified 12 percent with a 50 percent margin of error for theoretical approximation gives

$$d_e = \sqrt{\frac{0.18}{6.24}} = 0.17 \text{ in.} \quad (4.3 \text{ mm})$$

The ratio of inlet or supply pressure to average chamber pressure is found from

$$\frac{P_I}{P_c} = \frac{1}{\bar{p}} = \frac{A_e}{A_{I/2}} = \frac{d_e^2}{d_{I/2}^2} \quad (11)$$

Both \bar{p} and $\frac{P_I}{P_c}$ are simple linear relationships of areas or are related to the diameter squared for the two-hole design. Various diameters were selected from plots of these functions for further evaluation.

Nozzle area ratios were calculated from the selected nozzle throat diameter combinations. The allowable variation in nozzle exit ambient pressure was determined next--these nozzle exit ambient pressures are the chamber pressure for the inlet nozzle and the exhaust duct or room environmental pressure for the outlet nozzle.

A conical convergent and divergent nozzle was considered. The equations, tables, and charts of Reference 4 were used to make the calculations. The Summerfield criterion* was also used as a guide. The nozzle flow was assumed to be sonic at the throat and supersonic for a distance downstream to the location of a normal shock. The flow is assumed to be subsonic throughout the remaining nozzle length. The allowable pressure ratio for each set of nozzles is then used in Equation (9) to determine the frequency range of the set.

Consideration was then given to additional unmodulated holes in the chamber. The mechanical design was reviewed to determine the number and size of additional static pressure control nozzles that could be accommodated. Two was found to be the limit because of space and structural considerations. These openings are designated as holes 3 and 4 and their diameters by d_3 and d_4 . These holes may be used separately or in any combination as either an inlet, an outlet, or not at all. Blank (solid) nozzle inserts are provided for the latter option. The inlet pressure is considered to be the same at all inlet holes (although they could be operated independently at different pressures to give different performance). Each different multiple hole combination besides giving different performance also has different inlet supply pressure to chamber pressure ratios, P_I/P_c .

* Separation may occur when the ratio of the nominal exit pressure as computed from

$$\frac{A_e}{A_t} = \frac{\sqrt{\gamma} \left(\frac{2}{\gamma+1} \right)^{\frac{\gamma+1}{2(\gamma-1)}}}{\left(\frac{p_e}{p_c} \right)^{1/\gamma} \sqrt{\frac{2\gamma}{\gamma-1} \left[1 - \left(\frac{p_e}{p_c} \right)^{\frac{\gamma-1}{\gamma}} \right]}}$$

to ambient pressure is lower than 0.4 for conical divergent nozzles whose divergence half angle is of the order of 15 degrees, and for pressure ratios of the nozzle inlet pressure to the nozzle ambient pressure greater than 16.

An analysis was performed for each of the five additional combinations of the third and fourth holes in combination with first two holes. Dynamic amplitude versus frequency corresponding to flow areas was again calculated and the frequency corresponding to flow areas was again calculated and the frequency range of the various nozzles was determined for the various nozzle area ratios as before.

From these analyses the hole sizes and resultant pressure requirements were chosen and are given in Table 1.

TABLE 1. CALCULATED HOLE SIZES*

P_I/P_c	d_e in./mm	d_I in./mm	d_3 in./mm	d_4 in./mm
4.8	0.17/4.3	0.11/2.8	0	0
2	0.17/4.3	0.11/2.8	+0.10/2.54	0
1.1	0.17/4.3	0.11/2.8	+0.10/2.54	+0.10/2.54
2.4	0.17/4.3	0.11/2.8	+0.10/2.54	-0.10/2.54
8.1	0.17/4.3	0.11/2.8	-0.10/2.54	-0.10/2.54
6.4	0.17/4.3	0.11/2.8	-0.10/2.54	0

* where a + sign indicates the hole is being used as an inlet and a - sign indicates the hole is being used as an outlet.

The theoretical IM-SPG performance for the various hole combinations with hydrogen is shown in Figure 2. The curves were calculated using either Equation (3) or (4) and (8) for the various hole diameters in Table 1 throughout the specified frequency range from 15 Hz to 15 kHz. A summary of the curves at frequencies of 15 and 10,000 Hz is given in Table 2. Table 2 shows

TABLE 2. CALCULATED PEAK-TO-PEAK PRESSURE

P_I/P_c	$\hat{P}, \%$	
	Frequency, Hz	
	15	10,000
8.1	199.4	30.5
6.4	179.5	24.2
4.8	199.6	18
2.4	76.1	9.3
2.0	77.5	7
1.1	46.4	4.2

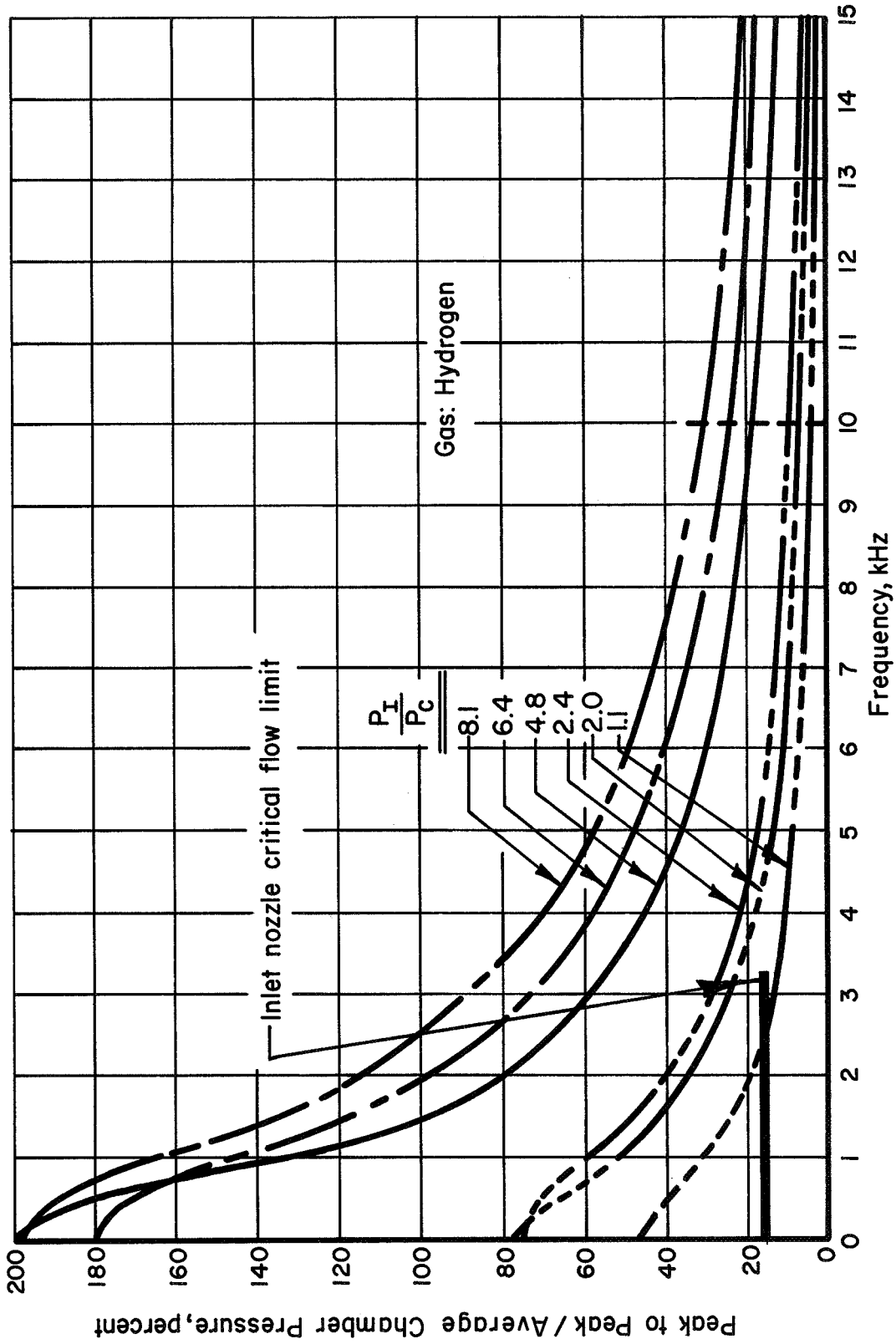


FIGURE 2. PERCENT PEAK-TO-PEAK PRESSURE TO CHAMBER PRESSURE VERSUS FREQUENCY FOR INLET-MODULATED SPG

that it is predicted that the IM-SPG design meets or exceeds both required \hat{p} specifications.

This performance has been maximized to give as large a dynamic amplitude over as large of a frequency range as possible at reasonable inlet pressures. Consequently, it was not always possible to operate with subsonic nozzle flow at the chamber entrance into the chamber by containment of the shock within the nozzle.

For instance, when only using a modulated inlet hole and the nominal outlet hole ($P_I/P_C = 4.8$), the shock is located near the nozzle exit as the sinusoidal pressure variation becomes zero, i.e., crosses the average pressure. As the fluctuation amplitude increases the shock recedes into the nozzle but critical flow is always maintained. However, when the fluctuation pressure drops below the average chamber pressure, the shock leaves the nozzle and the under-expanded flow enters the chamber. Similar conditions exist for $P_I/P_C = 6.4$ and 8.1 and possibly for part of $P_I/P_C = 2.4$ and for a very small region of $P_I/P_C = 2.0$. For $P_I/P_C = 1.1$, the shock is within the nozzle at all times but the nozzle is not choked at the lower frequencies.

Following the selection of nozzle throat and exit areas the nozzle design was completed. Calculations involving nozzle angles to determine nozzle overall lengths consistent with standard nozzle design practice and with some of the other SPG dimensions were made.

Mechanical Design

General. The mechanical design of the IM-SPG proved to be very complex. The desired design was to be a very adjustable and flexible design of high accuracy and mechanical strength capable of operating with a hazardous gas (hydrogen) at high pressure or vacuum conditions on pressure transducers and connecting passages of various shapes and sizes. The final mechanical design achieved all of these objectives.

The mechanical design is depicted in Figure 3. Basically it consists of a housing [7-1/2 in. (191 mm) x 4-1/8 in. (105 mm) x 6-1/2 in. (165 mm)] with a fixed in-place rotating shaft which is driven through a belt-pulley system by a variable-speed, servo-controlled motor. The chamber in which the sinusoidal pressure is generated also extends through the housing and bolts onto the housing through the outside seating flange. The rotating disk bolts onto the shaft. The chamber is positioned laterally in the direction of the holes in the disk relative to the disk by a lever-wedge mounted on the housing exterior and acting against the housing flange. Chamber position relative to the shaft centerline is limited to a small fraction of the distance between the shaft and chamber centerlines (analysis showed all expected hole sizes could be properly located in such a small change). An inlet gas tube extends through the housing and is positioned adjacent to the disk in line with the chamber modulated inlet nozzle. Clearance between the disk and inlet tube end is controlled by a differential screw. Gas flow from the chamber is through an outlet tube which screws into the chamber and exits through the housing. Gas escaping through the clearances on each side of the rotating disk is contained by the housing and exhausts out through an exit port. Both exit gas outlets are connected by piping to the ambient atmosphere. Gas leakage out along the

LEGEND

- ① Perforated disk
- ② SPG chamber body
- ③ Test transducer mounting adaptor
- ④ Monitor transducer mounting adaptor
- ⑤ Inlet nozzle
- ⑥ Outlet nozzle
- ⑦ Inlet tube
- ⑧ Outlet tube
- ⑨ Chamber positioning lever
- ⑩ Differential screw
- ⑪ Bearing housing
- ⑫ SPG housing
- ⑬ Magnetic pickup holder

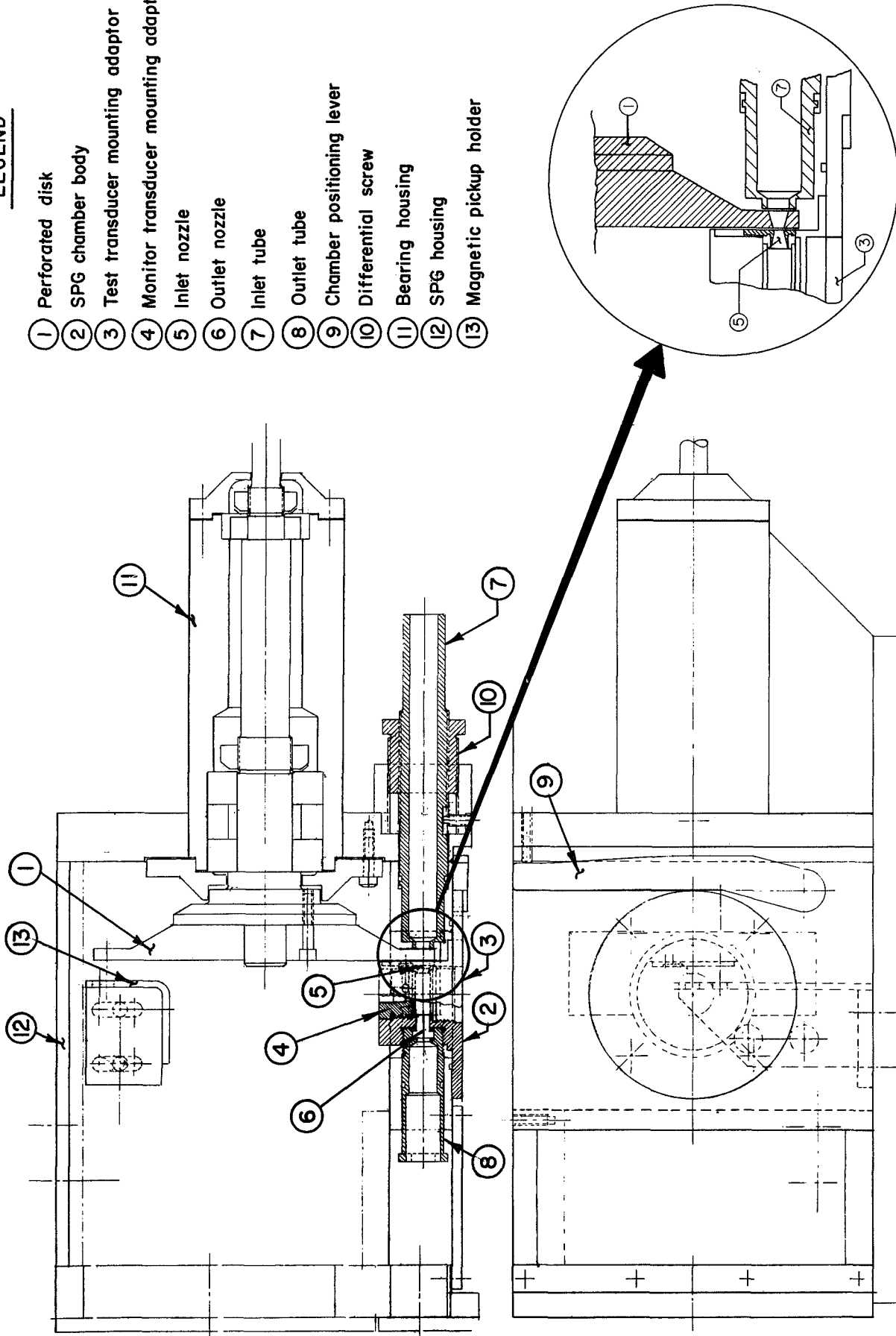


FIGURE 3. DRAWING OF INLET-MODULATED SINUSOIDAL PRESSURE GENERATOR

rotating shaft is prevented by labyrinth seals at each end of the shaft housing and by pressurizing the shaft housing to several atmospheres above the SPG housing pressure with an inert gas. The housing pressurizing gas is also used to lubricate the bearings by initially passing it through an oil mist lubricator.

Design Description. The ability to change chamber diameter is available in the final design. This was desired so that the highest frequencies could be obtained for each size of transducer. Chambers smaller than 3/4-inch (19.1 mm) diameter can be mounted and positioned into the SPG without modification simply by a bolting arrangement. The chamber resonant and usable frequencies* are inversely proportional to the chamber diameter. A chamber sized for calibrating a 3/4-inch (19.1 mm) or 1-inch (25.4 mm) transducer could not be tested to as high of a frequency as one designed for use with 1/4-inch (6.4 mm) to 1/16-inch (1.6 mm) transducers (whose frequency range is also usually inversely proportional to their diameter). Operating costs (gas consumption) of the SPG are also directly related to chamber size.

Besides providing the multiple chamber inlets and outlets (and their associated flow passages) of the unit to obtain a wide range of fluctuation-static pressure conditions, the ability to change the orifices is provided. The ability to change orifices rather than having them fixed or permanent (e.g., machined in the chamber) allows interchangeability of the various inlet and outlet nozzles. Thus, one can use different diameters for more flexible pressure conditions or insert blanks to eliminate any nozzle.

Because the holes in the rotating disk must be the same as the throat of the chamber inlet nozzle, the disk was designed so as to be removable from the rotating shaft to allow changing chamber and nozzle sizes. The accurately positioned shaft is mounted in superprecision bearings and permanently installed in the housing sleeve provided. One end of the shaft has a precision machined flange for affixing the disk. Axial runout of the disk surface during rotation is less than 0.0001 in. (2.5 μ m). Positioning of the chamber (including its perpendicularity in two directions) by the flat flange face and wedge-lever and of the inlet tube by the differential screw are of the accuracy of 0.001 in. (25 μ m). Differential screw adjustment is 0.0055 in. (0.14 mm) per revolution. All parts were designed such that any deflection or deformation would be less than 1/1000-inch (25 μ m) [1/10,000-inch (2.5 μ m) in most cases] at maximum load conditions.

Pressure transducers or their connection pieces are connected or mounted into the SPG chamber via a mounting adaptor. These adaptors are essentially plugs or cylinders with external threads for screwing into the SPG. They are machined internally so that each transducer or its connecting piece is flushed mounted to the SPG chamber surface. A similar mounting adaptor is used on the opposite side of the chamber to house the "standard" or monitor transducer. Thus, different "standard" transducers can also be used.

* Defined as that frequency which gives satisfactory performance for the evaluation being performed and is normally about 1/3 to 1/2 of the resonant frequency.

The housing serves to contain the hazardous gas and also to reduce vacuum pumping requirements. It has a removable top which is bolted on and sealed for providing access into the disk and monitor transducer. A side plate (bolted and sealed) covers a recess on the chamber flange side of the housing. The recess allows access to the SPG chamber exhaust tube which also serves as part of the chamber positioning mechanism. The downstream side of the housing opposite the shaft sleeve has two openings--one in the main housing to provide an exhaust for gas leakage through the disk clearance and one out of the recess for chamber gas exhaust. These holes were provided for working access and for alignment sighting purposes. A cover plate is used to provide exhaust piping connections. The housing side walls and bottom are of thick wall construction varying from 0.38-inch (9.65 mm) to 1.25-inch (31.75 mm). They serve as rigid stable surfaces for mounting and positioning the various components. Initially, the housing requirement complicated the design in several ways. Attempts were made to operate the housing fully pressurized in order to minimize any possible clearance effects and to reduce gas requirements. However, after much effort, no satisfactory dynamic seal suitable for operation with the rotating shaft at the high speeds [10-15,000 rpm] (167-250 Hz) or pressures [5000 psi] (34.5 MN/m^2) involved was found. Also, it was difficult to provide multiple chamber-multiple orifice capability with sufficient clearance for transducer connecting passages until low housing pressure operation was selected.

The unit was mounted on a stand designed to hold both the new IM-SPG and the Princeton University OM-SPG. The servo-controlled motor was mounted under the stand top such that it would drive both SPG's with the same belts. The stand is also of heavy construction for stability and vibration resistance. The stand top on which the SPG are attached is made of one-inch (25.4 mm) thick steel. The complete unit is shown in Figure 4.

IM-SPG CHARACTERIZATION SETUP

Following fabrication of the IM-SPG and assembly onto the stand with the OM-SPG, the unit was installed in one of the test cells at Battelle-Columbus's West Jefferson Site. The test cell was designed for hazardous testing with remote operation--it is normally used as a gaseous rocket motor test cell. Initially the SPG unit was to be located within the Battelle Aerothermal Research Facility. However, the necessary safety precautions for hydrogen operation required too many facility modifications and introduced operating difficulties which would have resulted in high costs. Similar difficulties were anticipated at several other sites considered at the main Battelle laboratory complex. The rocket motor test cells with their thickwall construction, separate control room, existing gas supply and control system, instrumentation connections, and remote location (which permits direct exhaust of the noisy and flammable gas) solved the location problem.

Description of System and Operation

A schematic drawing of the system is shown in Figure 5. System operation consists of setting the frequency to the desired value by adjusting

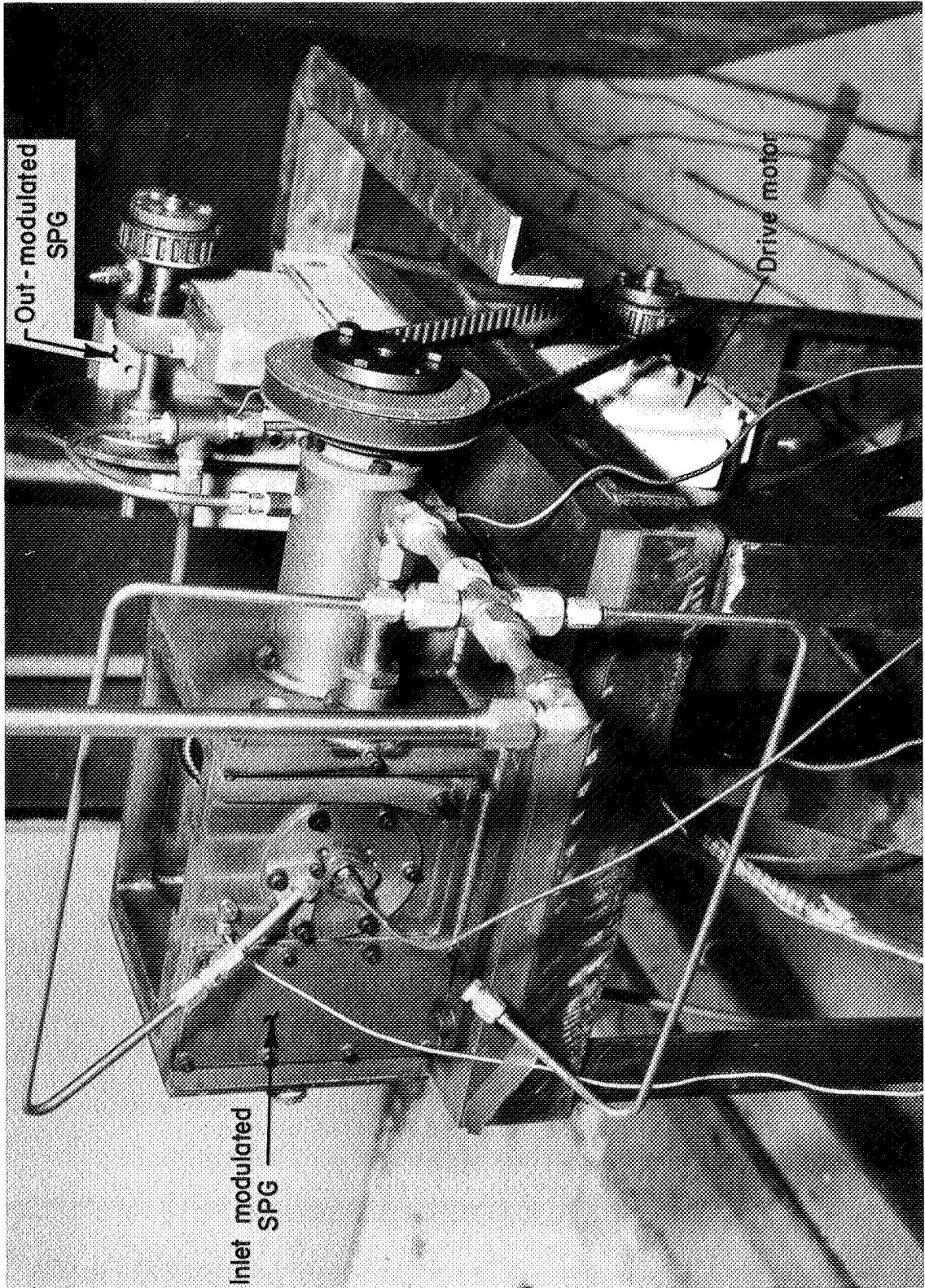


FIGURE 4. SINUSOIDAL PRESSURE GENERATOR

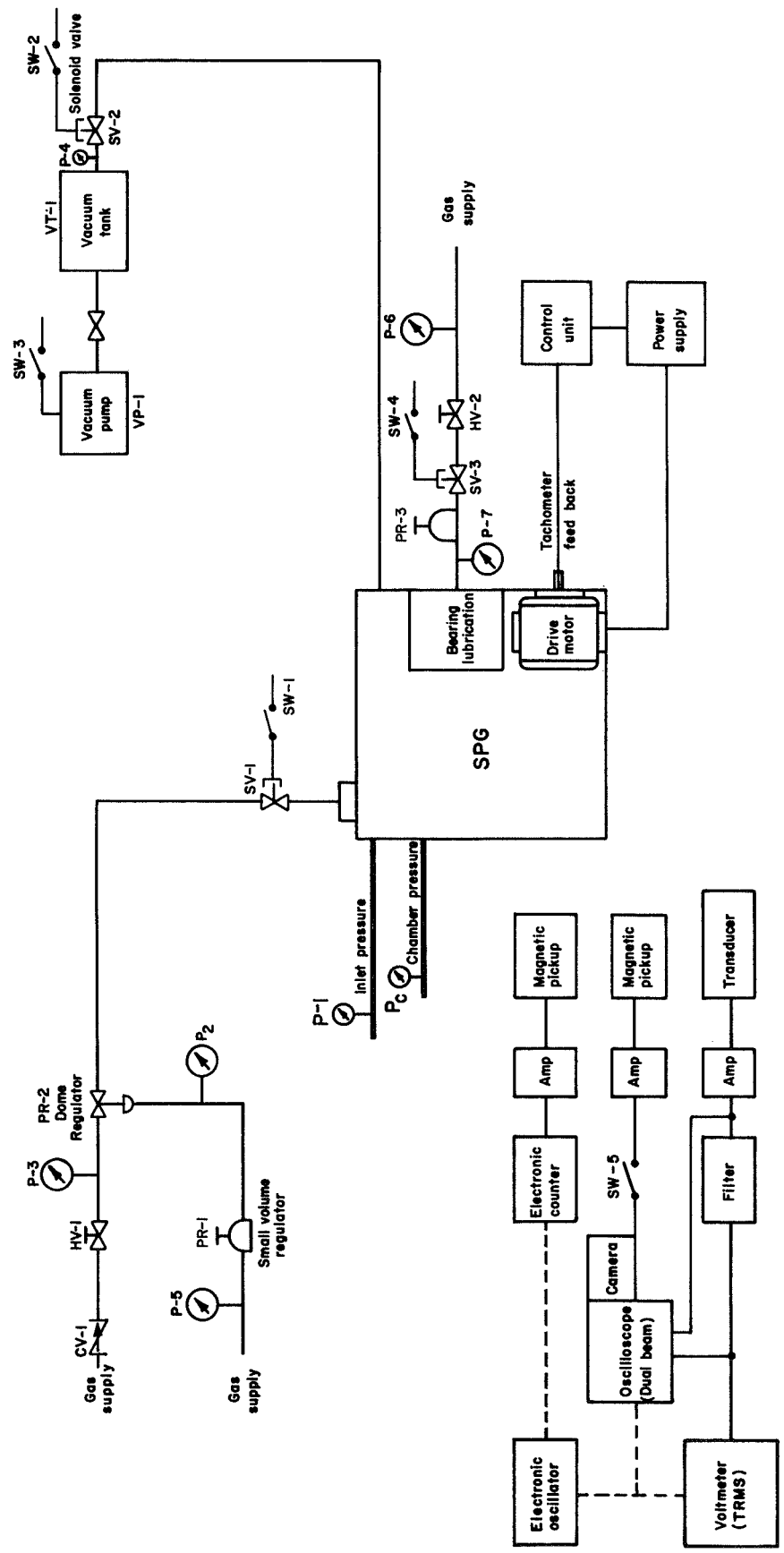


FIGURE 5. SCHEMATIC OF SINUSOIDAL PRESSURE GENERATOR SYSTEM

the ten-turn potentiometer on the Speed Control Head of the drive motor and monitoring the output of the Magnetic Pickup on the Electronic Counter. When the desired frequency is indicated on the counter, the solenoid valve SV-1 is actuated by operating switch SW-1 allowing hydrogen to flow to the SPG chamber. SPG inlet pressure is read on pressure gage P-1 and regulated by pressure regulator PR-2. Pressure regulator PR-2 is controlled by small volume regulator PR-1 whose pressure is read on pressure gage P-2. Gas supply pressure is read on pressure gage P-3. Test data are taken at the selected frequency and the test gas is shut off while the next test frequency is set by adjusting the Speed Control Head Potentiometer. This process of operation is repeated until the test series is completed.

Actual pressure transducer calibration can be performed in this manner or by sweeping through the desired frequency range and recording the transducer output on tape. Subatmospheric exhaust pressure required for low chamber pressures operation is obtained by operating switch SW-2. Switch SW-2 operates solenoid valve SV-2 which opens the exhaust duct to the vacuum tank VT-1. Tank VT-1 is evacuated by operating switch SW-3 of vacuum pump VP-1. Pressure in tank VT-1 is measured by pressure gage P-4. Depending on pressure conditions several tests can be obtained with tank VT-1. Evacuation of Tank VT-1 is accomplished in several minutes.

Lubrication of the SPG precision bearing is obtained by operating switch SW-4. Nitrogen gas passes through the oil mist unit to the bearing housing.

The working gas used in the tests was commercially-bottled hydrogen. A ten bottle manifold was used to minimize gas expansion temperature drop at the high mass flow rates required.

Piping was installed on both the chamber exhaust tube and the housing to vent the hydrogen out of the test cell.

The SPG was operated from the control room adjacent to the test cell. Visual and audio monitoring is possible.

Instrumentation and Data Recording

The instrumentation scheme presented in Figure 5 provided the necessary data to adequately determine the SPG performance (dynamic and static pressure and waveshape) up to 15,000 Hertz.

A quartz piezoelectric pressure transducer with a damped natural or ring frequency of 130 kHz was used to measure the SPG chamber dynamic pressure. (Several tests were also made with a quartz transducer with a ring frequency of over 400 kHz.) A charge amplifier was used to convert the transducer output to the order of volts. Several different filters were sometimes used to eliminate unwanted frequencies, including the transducer ring frequency when present, from the data. These filters were (1) a two-channel a.c. filter with option for a high pass frequency of 500 Hz and for either a low pass of 10 kHz or 20 kHz, (2) an adjustable filter that could be used as a band-pass (single low pass-single high pass) d.c. or a.c. filter incrementally from zero to 100 kHz or as a dual channel single filter

(either low pass or high pass on either channel in either mode), and (3) a single channel variable band-pass filter with adjustable upper and lower cutoff frequencies (20 Hz - 20 kHz). The signal, filtered or unfiltered, was read on a true rms voltmeter and recorded. Signals were also displayed on a dual beam oscilloscope and photographed. A dual beam scope was used to allow a filtered and unfiltered signal to be recorded when desired and to obtain waveshape information.

An instrument-laboratory-calibrated wide-range oscillator was used to help calibrate the system and its components for both frequency and amplification or attenuation factors before and after each test series. The frequency counter was calibrated in the Battelle Instrument Laboratory and was used to check the oscillator.

The inlet and chamber static pressure were measured with high accuracy gages (± 0.1 percent FS) and were visually noted and manually recorded. Several chamber static pressure measurements were also made with the quartz transducer.

IM-SPG CHARACTERIZATION RESULTS

The development and evaluation testing of the IM-SPG was performed over a range of nominal chamber pressures from 50 psia ($345 \text{ kN/m}^2\text{abs}$) to 300 psia ($2.07 \text{ MN/m}^2\text{abs}$) and over a range of frequencies from 0.75 kHz to 15 kHz. Two SPG configurations were tested, one inlet and one outlet, and two inlet and one outlet. The primary data of these tests were the ratio of inlet pressure to average chamber pressure, P_I/P_C , the ratio of peak-to-peak pressure to average chamber pressure, \hat{p} , and waveform. These results are discussed next.

Inlet Pressure to Average Chamber Pressure Ratio

The ratio of the inlet pressure to the bias or average chamber pressure determines the gas supply system pressure which must be maintained to produce any desired chamber pressure. For the first configuration tested where P_I/P_C was predicted to be 4.8, the average value of the test results was 5.4. P_I/P_C varied slightly with both pressure level and frequency. For normal operation the total change was less than ± 5 percent. For several of the tests where the clearance between the rotating disk and the gas supply inlet tube or the inlet nozzle was increased and/or decreased the nominal value variance increases to ± 10 percent.

For the second configuration where P_I/P_C was predicted to be 2.0, the average test result value was 2.2. The variances with pressure level and frequency and with clearance were essentially the same as for the first configuration.

These differences in predicted and measured values were expected and considered satisfactory. A simple one-dimensional flow model was used to calculate these values. No attempt was made to account for the complicated inlet flow region. In this region there are two flow splits in the nozzle, the clearances on each side of the disk. There may be complicated inertial and cross-stream viscous effects as the area changes due to the disk rotation. The nozzle flow discharge coefficient is not expected to be the same as that for the circular throat assumed as the shape changes during a cycle (similar to a convex lens most of the time). Also the area was assumed to vary sinusoidally which is only an approximation. Finally, the nozzle shocks were assumed to be normal with no obliqueness or boundary layer interactions.

The differences between the theoretical and experimental values for the second configuration was less than the first, 10 percent as compared to 12.5 percent.

This improvement is believed due to the effects of the third hole. It helps produce pressure in the chamber but does not have all of the complication of the variable inlet.

Oscillating Pressure Amplitude

The measured fluctuation pressure capability of the IM-SPG for the two configurations tested expressed as the ratio of peak-to-peak pressure to chamber pressure is given in Figure 6. The performance is shown as a wide, lined curve. The corresponding predicted dynamic performance curve, previously presented in Figure 2, is also given as is the associated values of P_T/P_C . Data from both development and evaluation tests are included. Most of the spread in the data was obtained during the tests where disk clearance effects were being investigated. Also some of the spread was caused by the uncertainty in the data reduction from the oscilloscope photographs. There was some spread due to pressure level effects. This was of the order of several percent. It varied with frequency with no trend perceived.

It is seen that the experimental results were in good agreement with the theoretical predictions. From these results it is concluded that the theoretical performance curves adequately represent the nominal performance of the IM-SPG.

The performance values given have all been for hydrogen operation. Dynamic amplitude for any other gas can be determined by using the proper value of the η in equation 9 or by multiplying the hydrogen performance curves of Figure 2 by the ratio of the η for the desired test gas to that of hydrogen. For helium and nitrogen the ratio values are 0.76 and 0.29, respectively. It should be noted that the variable frequency range of the gas varies with the speed of sound of the gas. Normally satisfactory performance is obtained at frequencies up to about 1/3 or 1/2 of the first resonant frequency of the chamber.

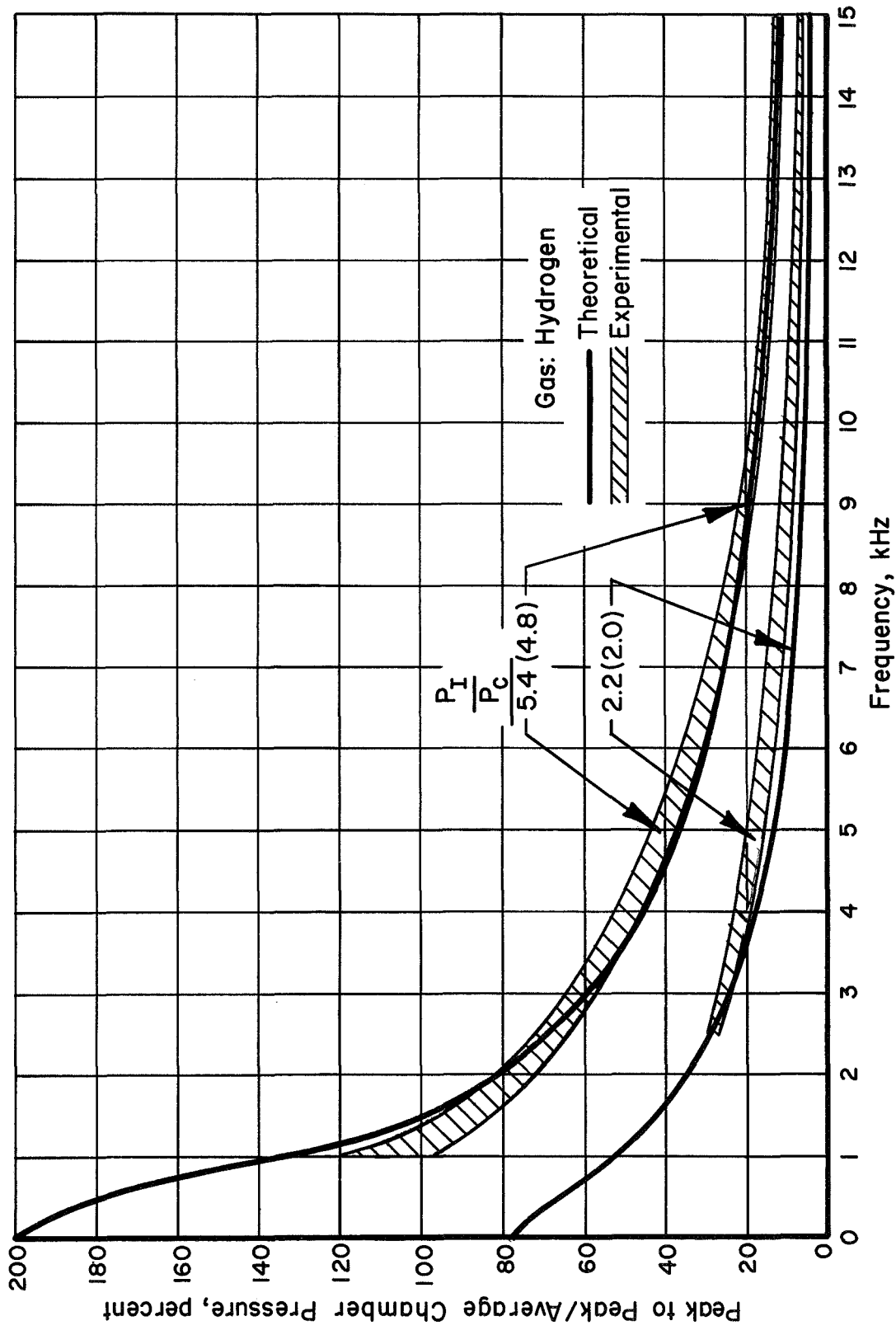


FIGURE 6. EXPERIMENTAL SINUSOIDAL PRESSURE GENERATOR PERFORMANCE

Waveform

The waveform of the IM-SPG chamber pressure transducer output signal was recorded by photographing oscilloscope traces. Waveform analysis consisted of visual inspection and electronic filtering.

In general, the waveform characteristics were the same as have been found in the OM-SPG and as have been discussed in detail in References (2) and (3). The waveform becomes distorted with increasing frequency and the distortion increases with increasing frequency. This is the most general characteristic and can be seen by examination of Figures 7, 8, and 9. Each part of the figures contains two signals. The unfiltered pressure transducer output signal is the bottom trace (except for Figure 8b) and the top trace is the same output after filtering.

The signal distortion did not change significantly with either pressure level (average chamber pressure) or with the SPG configuration (number of nozzles in use) as far as could be determined with this method of data recording and reduction. Figures 7d, 7c and 7f, 8c and 8d, 8f, 9a and 9b give comparisons of waveform at different average pressure levels for several different frequencies for one configuration (single inlet-single outlet). Sensitivity to pressure level was expected to be small for each configuration because the SPG operates on pressure differences. Thus, the expansion and compression processes operate over the same ratio, P_1/P_c , at 15 psia (103.5 kN/m²abs) and at 1500 psia (10.35 MN/m²abs). At these pressure levels the flow is still continuum flow and differences between these processes would be expected to be small. Comparisons of waveform for the two different configurations can be made with Figures 8 and 9 at different frequencies.

A more detailed view of a waveform is shown in Figure 7d while cycle-to-cycle variation can be seen in Figure 7e. In order to compare the waveform of the SPG output to a sinusoidal waveform, a picture of the filtered SPG output and a sinusoidal waveform from a signal generator was taken. These signals are shown in Figure 8b. From this comparison it can be seen that the fundamental waveshape of the SPG is essentially sinusoidal as desired. The phase relationship and amplitude relationships of the two waveforms have no significance.

The waveform distortion exhibits two general characteristics (1) harmonics or higher order content and (2) transducer ringing. The harmonic content is seen to be related to the driving frequency. The transducer ringing is a fixed frequency associated with the transducer.

The higher harmonics in the output signal appear to be multiples of the drive frequency more than of the chamber response modes, e.g., first tangential, first radial, first longitudinal or any of the combined modes. An oscillation disturbance appears at the top and bottom and on each side of the nominal response signal. This characteristic occurs at all frequencies and increases in amplitude with increasing frequency. It appears that these disturbances are related to driving phenomena, e.g., wheel-inlet orifice geometry which would be repeatable at each point on the cycle regardless of frequency. However, this may also be due to the "bunching" of higher and combined modes, i.e., various modes existing concurrently in the chamber, due to the low "Q" (sharpness of resonance) of the cylindrical chamber such as was shown possible in Reference 3.

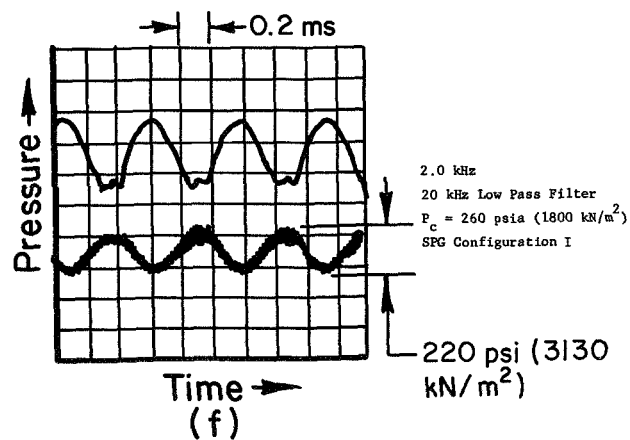
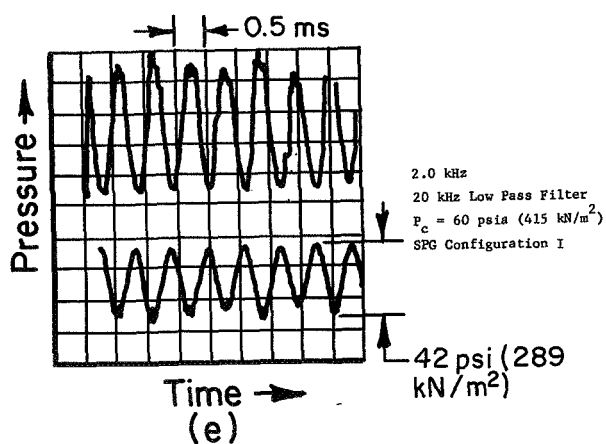
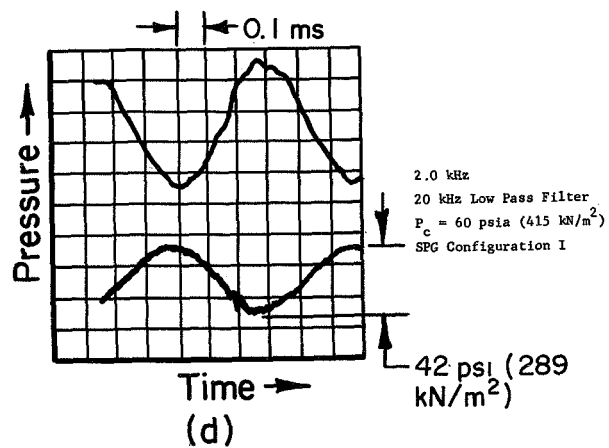
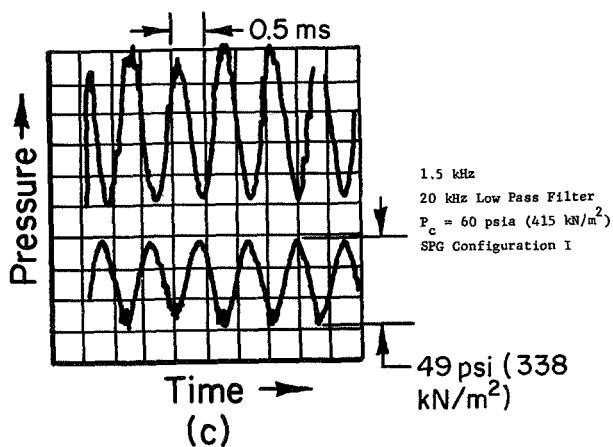
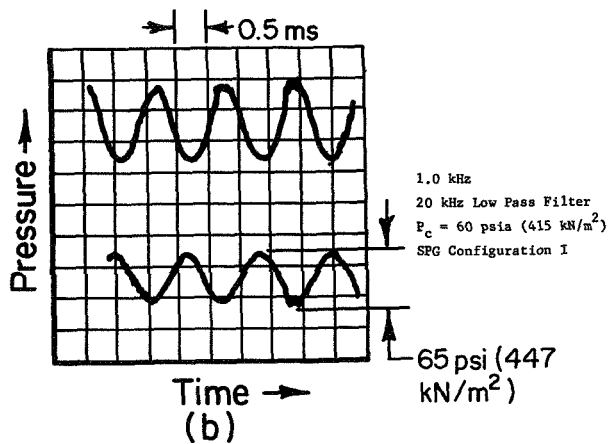
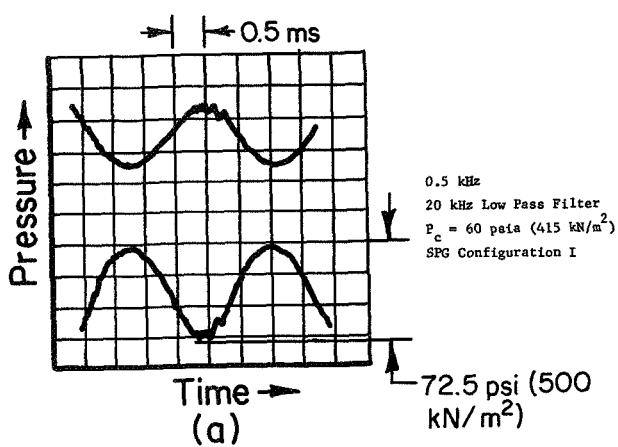


FIGURE 7. TYPICAL PRESSURE HISTORIES AT LOW FREQUENCIES AT VARIOUS PRESSURE LEVELS

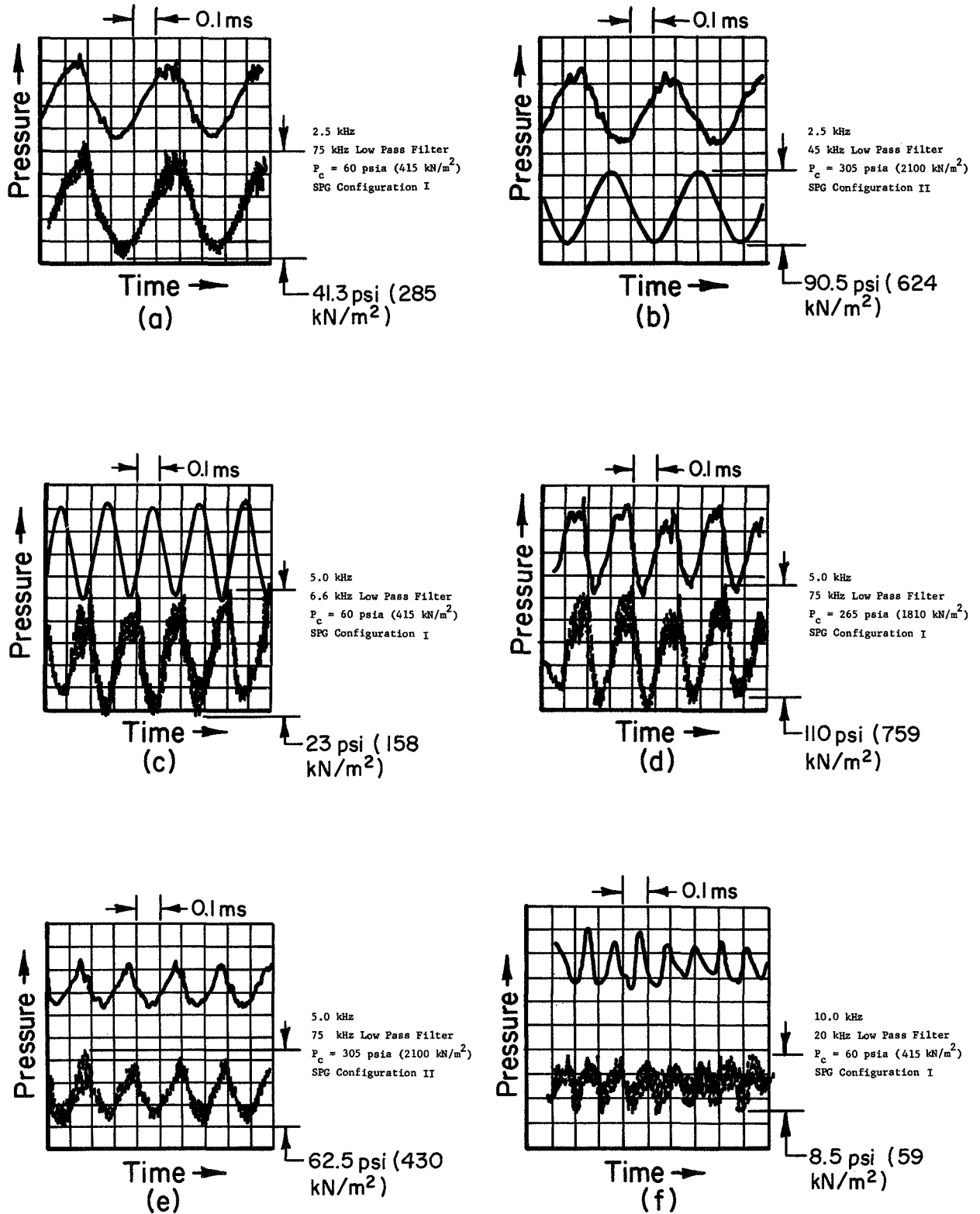


FIGURE 8. TYPICAL PRESSURE HISTORIES AT MEDIUM FREQUENCIES AT VARIOUS PRESSURE LEVELS

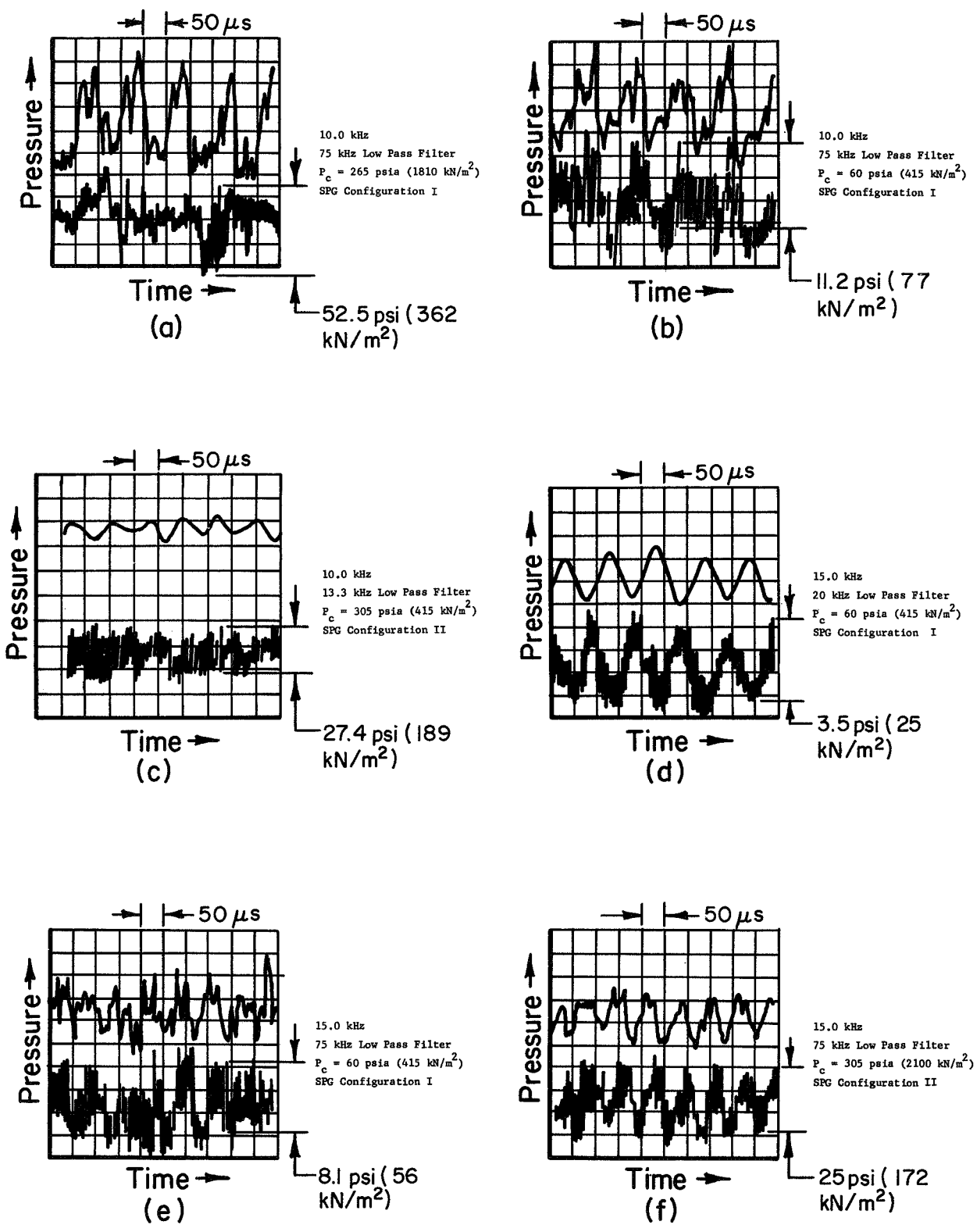


FIGURE 9. TYPICAL PRESSURE HISTORIES AT HIGH FREQUENCIES AT VARIOUS PRESSURE LEVELS

TABLE 3. TEST CONDITIONS

Figure	Frequency, kHz	Low Pass Filter Frequency, kHz	Average Chamber Pressure, psia/kN/m ²	SPG Configuration *
7a	0.5	20	60/415	I
7b	1.0	20	60/415	I
7c	1.5	20	60/415	I
7d	2.0	20	60/415	I
7e	2.0	20	60/415	I
7f	2.0	20	260/1800	I
8a	2.5	75	60/415	I
8b	2.5	45	305/2100	II
8c	5.0	6.6	60/415	I
8d	5.0	75	265/1810	I
8e	5.0	75	305/2100	II
8f	10.0	20	60/415	I
9a	10.0	75	265/1810	I
9b	10.0	75	60/415	I
9c	10.0	13.3	305/2100	II
9d	15.0	20	60/415	I
9e	15.0	75	60/415	I
9f	15.0	75	305/2100	II

* Configuration I corresponds to one inlet-one outlet ($P_I/P_c = 4.8$) and Configuration II corresponds to two inlet-one outlet ($P_I/P_c = 2.0$).

The transducer ringing occurs throughout a chamber pressure cycle. The ringing amplitude also increases with increasing frequency. It should be noted that the ringing amplitude portion on the output signal is much larger than the amplitude of the high frequency pressure component or high rate of change of pressure component actually existing in the chamber. This is because the transducer is responding at resonance. At resonance the amplification of the transducers is 16 for the 130 kHz type transducer and 7 for the 400 kHz type transducer. These values were determined by previous calibrations in a shock tube. Thus, a relatively small high frequency or high time rate of change pressure is existent but it is causing a large distortion in the transducers' output. Ringing occurred with both transducers (130 kHz and 400 kHz). Several possible explanations for this high frequency pressure component are that it is due to the higher chamber combined mode responses coupled to the driving frequency or that large amplitude pressure waves or shock waves which certainly contain high frequency components are present. The latter pressure conditions could come from the inlet nozzle flow into the chamber being under-expanded and subsequently shocking, or from oscillating oblique shocks within the over-expanded nozzle flow or from boundary layer interactions.

Aerodynamic or fluid noise resulting from the Reynolds stresses or shear forces that are a property of turbulent flow could be a driving mechanism to higher coupled modes. Fluid noise is normally contained between the frequencies of 1000 Hz and 10,000 Hz and is therefore not expected to directly excite ringing.

From the above, it is seen that the waveform distortion increases with the fundamental or driving frequency. However, the waveform maintained the fundamental or sinusoidal form even with the imposed distortion. It did not degenerate into noise or lose the dominance of its single driving frequency. The distortion in the chamber pressure is less than indicated in the transducer output signal because of amplification at transducer resonance. Accounting for the transducer resonance amplification effect would reduce the observed distortion level. Thus, the IM-SPG can be used to evaluate pressure sensing systems at the drive frequency over wide ranges of pressure levels, amplitudes, and frequency.

SUMMARY OF RESULTS

A sinusoidal pressure generator has been designed and constructed. Preliminary development and evaluation tests were made and the following results were found:

- (1) The IM-SPG concept was extended to additional operating modes (configurations) by the addition of extra flow passages.
- (2) Tests confirmed the concept of using additional holes to change mean pressure levels.
- (3) Specified performance was exceeded by 50 percent. Excellent agreement between the theoretical predicted pressures and those obtained experimentally was found. A ratio of peak-to-peak

pressure to average chamber pressure of 0.18 was obtained at 10 kHz. This is considerably above the required specification of 0.12 at 10 kHz. At 1 kHz the ratio of 1.20 was obtained and at 15 kHz the ratio was 0.12. Values up to 1.65, 0.31, and 0.20 are predicted to be obtainable at 1, 10, and 15 kHz, respectively. From the test results it was concluded that the theoretical performance curves adequately represent the nominal performance of the IM-SPG and therefore the specified ratio of 1.0 at 15 Hz would also be met or exceeded.

- (4) The waveform of the transducer output signal was distorted but consisted primarily of the driving frequency fundamental sinusoid. Distortion was found to increase with increasing frequency. Distortion effects would limit the IM-SPG in its present form as a dynamic pressure transducer calibrator to the order of several thousand Hertz. However, the IM-SPG is suitable for less stringent evaluation tests of pressure measuring systems up to 15,000 Hertz.

RECOMMENDATIONS

The conditions of nozzle over-expansion and under-expansion with various shock wave conditions is a likely source of distortion producing mechanisms.

Another highly suspected cause of signal distortion is the changing throat area, size, shape, and location at the inlet nozzle. The result is that essentially a flow jet through a crescent shaped area at the side of the divergent section exists at times during a cycle and is at an angle relative to the nozzle centerline. The divergent section always remains conical and does not vary throughout a cycle like the throat.

Other flow effects that may have to be investigated are flow acceleration or unsteady effects, exit nozzle acoustic impedance and phasing effects between the two chamber nozzles, relative size of nozzles to chamber dimension, flow reflections back up the inlet tube from off the wheel, expansion (rarefaction) effects of clearance separation and flow on main core flow going into SPG.

It is recommended that further development of the Inlet-Modulated Sinusoidal Pressure Generator be undertaken. This effort should be primarily directed at improving the pressure waveform and should include the following:

- (1) Signal analyses should be performed to determine the frequencies and amplitudes of waveform distortion and to separate any transducer or related electronic system effects.
- (2) Distortion causes should be identified and related to driving or generating mechanisms.
- (3) Modifications should be incorporated into the IM-SPG to eliminate or suitably reduce the distortion. The effects of these modifications should be verified by performance tests.

REFERENCES

- (1) Robinson, R. E., and Liu, C. Y., "Resonant Systems for Dynamic Transducer Evaluations", NASA CR-72435 (August 31, 1968).
- (2) Bentley, W. C., and Walter, J. J., "Dynamic Response Testing of Transient Pressure Transducers for Liquid Propellant Rocket Combustion Chambers", Princeton University Aeronautical Engineering Report No. 595g (June, 1963).
- (3) Carwile, C. L., "An Analytical and Experimental Study of the Response of a Small Chamber to Forced Oscillations", Aeronautical Engineering Report No. 595d, Princeton University (October 15, 1962).
- (4) Ames Research Staff, "Equations, Tables, and Charts for Compressible Flow", NACA Report 1135 (1953).

APPENDIX A

DERIVATIONS OF EQUATIONS
GOVERNING THE OPERATION OF THE
SINUSOIDAL PRESSURE GENERATOR

Mass flow-modulated SPG's of the type under consideration are designed on the following conditions: (1) the modulating frequency is below system resonance frequency and (2) the flows through the modulating orifices are at critical flow condition. Condition (1) means that pressure variation in the gas produced by the modulation will be quickly transmitted to the entire gas by the high-speed acoustic wave so that the gas condition can be treated as a uniform medium at any instant. This makes it possible to analyze the SPG by using the gas flow relation while the detailed wave propagation in the gas can be ignored. Condition (2) results in controllable modulation with no interaction between modulating flow and downstream pressure.

Based on the above two conditions, an SPG as shown in Figure A-1 can be analyzed as follows.

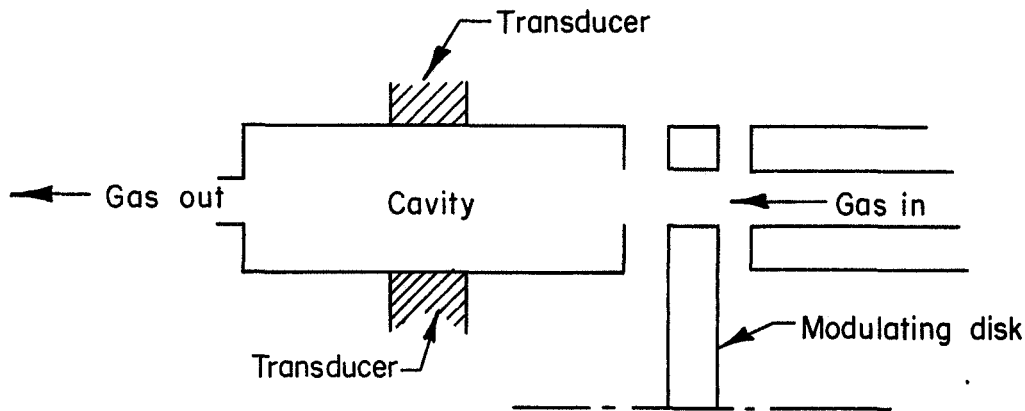


FIGURE A-1. INLET-MODULATED SINUSOIDAL PRESSURE GENERATOR

From conservation of mass, the time rate of mass increase in the chamber \dot{m} is related to the inlet flow rate \dot{m}_{in} and outgoing flow rate \dot{m}_{out} by

$$\dot{m} = \dot{m}_{in} - \dot{m}_{out} \quad .$$

For perfect gas at critical flow

$$\dot{m}_{in} = C_D \alpha A_i p_o$$

$$\dot{m}_{out} = C_D \alpha A_e p$$

$$\dot{m} = \frac{V}{RT_o} \dot{p}$$

$$\alpha^2 = \frac{g_c \gamma}{RT_o} \left(\frac{2}{\gamma+1} \right)^{(\gamma+1)/(\gamma-1)}, \text{ a constant,}$$

Combining the above relations yields

$$\dot{p} = \frac{\alpha RT_o}{V} (A_i p_o - A_e p),$$

or

$$\frac{\dot{p}}{p_o} = \eta (A_i - A_e \frac{p}{p_o}), \quad (A-1)$$

where

$$\eta = \frac{\alpha RT_o}{V} = \frac{C}{V} \left(\frac{2}{\gamma+1} \right)^{(\gamma+1)/2(\gamma-1)}, \text{ a constant} \quad (A-2)$$

$$C = (g_c \gamma RT_o)^{\frac{1}{2}}, \text{ sonic velocity at gas supply.}$$

Denoting $p/p_o = p^*$, Equation (A-1) becomes

$$\dot{p}^* = \eta (A_i - A_e p^*) \quad (A-3)$$

Equation (A-3) is the governing equation for an ideal SPG. The modulation of pressure can be achieved by varying the exit area A_e and/or the inlet area A_i . The Princeton University SPG operated at Battelle for NASA is equipped with an outlet-modulation device. From Equation (A-3), it is seen that exit modulation causes interaction with the pressure response because of the term $A_e p^*$. Inlet area modulation avoids the complications of exit modulation (the exit area is constant).

Describing the pressure variation taking place around an average or bias pressure \bar{p} which is time independent as

$$p^* = \bar{p} + \tilde{p} \quad , \quad (A-4)$$

and introducing it into Equation (A-3) gives

$$\dot{\tilde{p}} + \eta A_e \tilde{p} = \eta (A_i - A_e \bar{p}) \quad (A-5)$$

If the inlet area is made of two types of openings, constant area openings and variable or modulated openings as described by

$$A_i = \bar{A}_i + A_i \quad , \quad (A-6)$$

with
$$\bar{A}_i = A_e \bar{p} \quad (A-7)$$

Equation (A-7) relates constant flow areas to average chamber pressure. It assumes all inlet areas are at the same upstream pressure and has to be modified when not so set.

Equation (A-5) becomes

$$\dot{\tilde{p}} + \eta A_e \tilde{p} = \eta \bar{A}_i \quad . \quad (A-8)$$

A sinusoidal pressure variation about an average pressure which is what is desired is described by

$$\tilde{p} = \tilde{p}_{amp} \sin \omega t \quad (A-9)$$

Combining Equations (A-8) and (A-9) yields

$$\begin{aligned}\tilde{A}_i &= A_e \tilde{p}_{\text{amp}} \sin \omega t + \frac{\omega}{\eta} \tilde{p}_{\text{amp}} \cos \omega t \\ &= \tilde{p}_{\text{amp}} \left(A_e^2 + \frac{\omega^2}{\eta^2} \right)^{\frac{1}{2}} \sin \left[\omega t + \tan^{-1} \left(\frac{\omega}{\eta A_e} \right) \right]\end{aligned}\tag{A-10}$$

Thus, the variable inlet area for a sinusoidal pressure variation is a sinusoidal area variation. Its physical size or amplitude is

$$\tilde{A}_{i(\text{amp})} = \tilde{p}_{\text{amp}} \left(A_e^2 + \frac{\omega^2}{\eta^2} \right)^{\frac{1}{2}} .\tag{A-11}$$

For very high frequency, Equation (A-11) gives

$$\tilde{p}_{\text{amp}} = \eta \tilde{A}_{i(\text{amp})} / \omega\tag{A-12}$$

APPENDIX B

APPROXIMATE SOLUTION ACCURACY

The choice of when to use the more convenient Equation (A-12) as the approximation for the more complex Equation (A-11) can be based upon the error, ϵ , one would accept or the accuracy desired. The relationship for this error and the frequency at which it occurs is related by:

$$\frac{\eta_e^A}{\omega} = (1 \pm \epsilon) \frac{\frac{\eta_e^A}{\omega}}{\sqrt{1 + \left(\frac{\eta_e^A}{\omega}\right)^2}}, \quad (B-1)$$

then

$$\sqrt{1 + \left(\frac{\eta_e^A}{\omega}\right)^2} = 1 \pm \epsilon,$$

or

$$\frac{\eta_e^A}{\omega} = \frac{\eta_e^A}{2\pi f} = \sqrt{(1 \pm \epsilon)^2 - 1} = \sqrt{\epsilon^2 \pm 2\epsilon},$$

yielding

$$f = \frac{\eta_e^A}{2\pi} \frac{1}{\sqrt{\epsilon^2 \pm 2\epsilon}} \quad (B-2)$$

Thus, if it is desired that the calculation should not be in error by more than 1 percent, the high frequency approximating Equation (A-12) can be used in place of Equation (A-11) for hydrogen and an exit area of 0.0227 in.² [12 mm²] (d = 0.17) [4.3 mm] down to a frequency of

$$f = \frac{2.5 \times 10^5}{\text{in.}^2\text{-sec}} \frac{0.0227 \text{ in.}^2\text{-cycle}}{2\pi \text{ rad}} \times \frac{1}{\sqrt{(0.01)^2 + 2(0.01)}}$$

$$= 6.35 \times 10^3 \text{ Hz}$$

For a 5 percent error

$$f = 2.81 \times 10^3 \text{ Hz} \quad .$$

Corresponding values for helium and nitrogen are:

	f, Hz	
	He	N ₂
$\epsilon = 0.01$	4.95×10^3	1.775×10^3
$\epsilon = 0.05$	2.19×10^3	0.786×10^3

DISTRIBUTION LIST

Dr. R. J. Priem MS 500-204 (2) NASA-Lewis Research Center 21000 Brookpark Road Cleveland, Ohio 44135	E. W. Conrad MS 500-204 NASA-Lewis Research Center 21000 Brookpark Road Cleveland, Ohio 44135	D. Harrje Princeton University James Forrestal Research Center P. O. Box 710 Princeton, New Jersey 08540
Normal T. Musial NASA-Lewis Research Center 21000 Brookpark Road Cleveland, Ohio 44135	Dr. E. K. Dabora University of Connecticut Aerospace Department Storrs, Connecticut 06268	T. Inouye Code 4581 U. S. Naval Weapons Center China Lake, California 93555
Library (2) NASA-Lewis Research Center 21000 Brookpark Road Cleveland, Ohio 44135	O. W. Dykema Aerospace Corporation P. O. Box 95085 Los Angeles, California 90045	R. D. Jackel, 429 Office of Naval Research Navy Department Washington, D. C. 20360
Report Control Office NASA-Lewis Research Center 21000 Brookpark Road Cleveland, Ohio 44135	G. W. Elverum TRW Systems 1 Space Park Redondo Beach, California 90278	R. B. Lawhead Rocketdyne, a Division of North American Aviation 6633 Canoga Avenue Canoga Park, California 91304
NASA Representative (6) NASA Scientific and Technical Information Facility P. O. Box 33 College Park, Maryland 20740	R. Edse Ohio State University Dept. of Aeronautical and Astronautical Engineering Columbus, Ohio 43210	R. S. Levine, Code RPL NASA Headquarters 6th & Independence Avenue, S.W. Washington, D. C. 20546
V. Agosta Brooklyn Polytechnic Institute Long Island Graduate Center Route 110 Farmingdale, New York 11735	G. M. Faeth The Pennsylvania State University Mechanical Engineering Department 207 Mechanical Engineering Blvd. University Park, Pennsylvania 16802	Ted Male MS 500-209 NASA-Lewis Research Center 21000 Brookpark Road Cleveland, Ohio 44135
B. P. Breen Dynamic Science, a Division of Marshall Industries 1900 Walker Avenue Monrovia, California 91016	G. D. Garrison Pratt and Whitney Aircraft Florida Research and Development Center P. O. Box 2691 West Palm Beach, Florida 33402	J. M. McBride Aerojet-General Corporation P. O. Box 15847 Sacramento, California 95809
Thomas J. Chew AFRPL (RPPZ) Edwards, California 93523	M. Gerstein Dept. Mechanical Engineering University of Southern California University Park Los Angeles, California 90007	P. D. McCormack Dartmouth University Hanover, New Hampshire 03755
T. W. Christian Chemical Propulsion Information Agency 8621 Georgia Avenue Silver Spring, Maryland 20910	I. Glassman Princeton University James Forrestal Research Center P. O. Box 710 Princeton, New Jersey 08540	C. E. Mitchell Colorado State University Fort Collins, Colorado 80521
R. M. Clayton Jet Propulsion Laboratory California Institute of Technology 4800 Oak Grove Drive Pasadena, California 91103	Richard W. Haffner Air Force Office of Scientific Research 1400 Wilson Boulevard Arlington, Virginia 22209	P. S. Myers University of Wisconsin Mechanical Engineering Department 1513 University Avenue Madison, Wisconsin 53705

J. A. Nestlerode
Rocketdyne, a Division of
North American Aviation
6633 Canoga Avenue
Canoga Park, California 91304

J. A. Nicholls
University of Michigan
Aerospace Engineering
Ann Arbor, Michigan 48104

James C. O'Hara
Tulane University
Department of Mechanical
Engineering
New Orleans, Louisiana 70118

A. K. Oppenheim
University of California
Department of Aeronautical
Sciences
6161 Etcheverry Hall
Berkeley, California 94720

J. R. Osborn
Purdue University
School of Mechanical Engineering
Lafayette, Indiana 47907

Dr. K. Ragland
University of Wisconsin
Mechanical Engineering Department
Madison, Wisconsin 53705

Dr. A. A. Ranger
Purdue University
School of Aeronautics, Astronautics
and Engineering Sciences
Lafayette, Indiana 47907

F. H. Reardon
Sacramento State College
School of Engineering
6000 J. Street
Sacramento, California 95819

B. A. Reese
Purdue University
School of Mechanical Engineering
Lafayette, Indiana 47907

R. J. Richmond R-Pand VE-PA
NASA George C. Marshall
Space Flight Center
Huntsville, Alabama 35812

J. H. Rupe
Jet Propulsion Laboratory
California Institute of
Technology
4800 Oak Grove Drive
Pasadena, California 91103

Dr. R. F. Sawyer
University of California
Mechanical Engineering,
Thermal Systems
Berkeley, California 94720

K. Scheller
ARL (ARC)
Wright Patterson Air Force Base
Dayton, Ohio 45433

Roger A. Strehlow
University of Illinois
Aeronautical Engineering
Department
Urbana, Illinois 61801

J. G. Thibadaux
NASA Manned Spacecraft Center
Houston, Texas 77058

T. P. Torda
Illinois Institute of
Technology
Room 200 M.H.
3300 S. Federal Street
Chicago, Illinois 60616

T. Y. Toong
Massachusetts Institute of
Technology
Department of Mechanical
Engineering
Cambridge, Massachusetts 02139

Richard Weiss
AFRPL
Edwards, California 93523

W. W. Wharton AMSMI-RKL
U. S. Army Missile Command
Redstone Arsenal, Alabama 35808

F. A. Williams
University of California
Aerospace Engineering Department
P. O. Box 109
LaJolla, California 92038

L. M. Wood
Bell Aerosystems Company
P. O. Box 1
Mail Zone J-81
Buffalo, New York 14205

B. T. Zinn
Georgia Institute of Technology
Aerospace School
Atlanta, Georgia 30332

Library
Goddard Space Flight Center (NASA)
Greenbelt, Maryland 20771

Library
NASA John F. Kennedy Space Center
Cocoa Beach, Florida 32931

Library
NASA Langley Research Center
Langley Station
Hampton, Virginia 23365

Library
NASA Manned Spacecraft Center
Houston, Texas 77001

Library
NASA George C. Marshall
Space Flight Center
Huntsville, Alabama 35812

Library
Jet Propulsion Laboratory
4800 Oak Grove Drive
Pasadena, California 91103

Library
NASA Flight Research Center
P. O. Box 273
Edwards, California 93523

Library
NASA Ames Research Center
Moffett Field, California 94035

TISIA
Defense Documentation Center
Cameron Station
Building 5
5010 Duke Street
Alexandria, Virginia 22314

Office of Assistant Director
(Chemical Technology)
Office of the Director of
Defense Research & Engineering
Washington, D. C. 20301

D. E. Mock
Advanced Research Projects Agency
Washington, D. C. 20525

Dr. H. K. Doetsch
Arnold Engineering Development Ctr
Air Force Systems Command
Tullahoma, Tennessee 37389

Library
Air Force Rocket Propulsion
Laboratory (RPR)
Edwards, California 93523

Library
Air Force Rocket Propulsion
Laboratory (RPM)
Edwards, California 93523

Library
Bureau of Naval Weapons
Department of the Navy
Washington, D. C.

Library
Director (Code 6180)
U. S. Naval Research Laboratory
Washington, D. C. 20390

APRP (Library)
Air Force Aero Propulsion
Laboratory
Research & Technology Division
Air Force Systems Command
United States Air Force
Wright-Patterson AFB, Ohio 45433

Technical Information Department
Aeronutronic Division of
Philco Ford Corporation
Ford Road
Newport Beach, California 92663

Library-Documents
Aerospace Corporation
2400 East El Segundo Boulevard
Los Angeles, California 90045

Library
Bell Aerosystems, Inc.
Box 1
Buffalo, New York 14205

Report Library, Room 6A
Battelle Memorial Institute
505 King Avenue
Columbus, Ohio 43201

D. Suichu
General Electric Company
Flight Propulsion Laboratory
Department
Cincinnati, Ohio 45215

Library
Ling-Temco-Vought Corporation
P. O. Box 5907
Dallas, Texas 75222

Marquardt Corporation
16555 Saticoy Street
Box 2013 - South Annex
Van Nuys, California 91409

P. F. Winternitz
New York University
University Heights
New York, New York

I. Forsten
Picatinny Arsenal
Dover, New Jersey 07801

R. Stiff
Propulsion Division
Aerojet-General Corporation
P. O. Box 15847
Sacramento, California 95803

Library, Department 596-306
Rocketdyne, Division of
North American-Rockwell Inc.
6633 Canoga Avenue
Canoga Park, California 91304

Library
Stanford Research Institute
333 Ravenswood Avenue
Menlo Park, California 94025

Library
Susquehanna Corporation
Atlantic Research Division
Shirley Highway & Edsall Road
Alexandria, Virginia 22314

STL Technical Library Document
Acquisitions
TRW System Group
1 Space Park
Redondo Beach, California 90278

Dr. David Altman
United Aircraft Corporation
United Technology Center
P. O. Box 358
Sunnyvale, California 94088

Library
United Aircraft Corporation
Pratt & Whitney Division
Florida Research & Development
Center
P. O. Box 2691
West Palm Beach, Florida 33402

Dr. Marshall C. Burrows MS 6-1
NASA-Lewis Research Center
21000 Brookpark Road
Cleveland, Ohio 44135

J. J. Kramer MS 7-1
NASA-Lewis Research Center
21000 Brookpark Road
Cleveland, Ohio 44135

D. R. Englund MS 77-1
NASA-Lewis Research Center
21000 Brookpark Road
Cleveland, Ohio 44135